Journal of King Saud University - Science 36 (2024) 103369

HOSTED BY

Contents lists available at ScienceDirect

Journal of King Saud University - Science

journal homepage: www.sciencedirect.com

Simple biotic; spinel $CoFe_2O_4$ nanosphere for textile pollutant removal by photoresponsivity process and anti-microbial analysis

M. Abdul Kapur [a], M. Kaviya Devi [a], R. Janani [a], J. Prasanna [a,*], N. Arumugam [b], Sinouvassane Djearamane [c,d,**], Ling Shing Wong [e], Saminathan Kayarohanam [f]

[a] PG and Research Department of Microbiology, Vivekanandha College of Arts and Sciences for Women (Autonomous), Elayampalayam, Namakkal 637205, Tamil Nadu, India
[b] Department of Chemistry, School of Chemical Sciences, University of Madras, Chennai, Tamil Nadu, India
[c] Department of Allied Health Sciences, Faculty of Science, University Tunku Abdul Rahman, Jalan University, Bandar Barat, Kampar 31900, Malaysia
[d] Biomedical Research Unit and Lab Animal Research Centre, Saveetha Dental College, Saveetha Institute of Medical and Technical Sciences, Chennai 602 105, India
[e] Faculty of Health and Life Sciences, INTI International University, Nilai 71800, Malaysia
[f] Faculty of Bio-economics and Health Sciences, University Geomatika Malaysia, Kuala Lumpur 54200, Malaysia

ARTICLE INFO

Keywords:
$CoFe_2O_4$ nanosphere
XRD
SEM and TEM
Rhizophora mucronata Leaf

ABSTRACT

This study focuses on the development and characterization of a biotic spinel $CoFe_2O_4$ nanosphere, synthesized using *Rhizophora mucronata leaf*, for textile pollutant removal via a photoresponsive process. The structure, morphology, and composition of the nanosphere were analyzed using X-ray diffraction (XRD), scanning electron microscopy (SEM), transmission electron microscopy (TEM), and Fourier-transform infrared spectroscopy (FTIR). The study also investigates the antimicrobial properties of the nanosphere to explore its potential in inhibiting harmful microorganisms in the textile industry. The research aims to provide insights into the feasibility of using $CoFe_2O_4$ nanospheres for efficient and eco-friendly textile pollutant removal and microbial control.

1. Introduction

The global production of dyes and pigments is estimated to reach 700,000 tonnes annually, leading to the continuous release of dye effluents into aquatic environments. These effluents are highly toxic, potentially carcinogenic, and mutagenic, posing serious health risks and disrupting ecological balance. The stability of dyes against light, temperature, and chemicals makes them persistent in the environment, challenging existing water and wastewater treatment technologies. To address these challenges, nanomaterials such as nano-adsorbents, nanofibers, and nano-photocatalysts offer promising solutions (Umar et al., 2023; Kavaz et al., 2019; Kavaz et al., 2021; Umar et al., 2024; Shaheen et al., 2020).

Methylene Blue (MB), a highly stable and soluble cationic dye, poses significant environmental threats due to its toxic and carcinogenic properties. Transition-metal ferrite nanocomposites (MFe_2O_4), incorporating elements such as Co, Cu, Mn, and Ni, have garnered interest for their applications in heterogeneous catalysis and environmental remediation (Pelino et al., 1994; Issa et al., 2013; Naseri et al., 2010; Charan and Shahi, 2016; Malinowska et al., 2020). These nanocomposites, particularly ferrites, exhibit photocatalytic properties, making them suitable for various industrial processes and enhancing efficiency through the spinel crystal arrangement and frequency gap (Kumar et al., 2017; Jia et al., 2012).

Despite their potential, studies on pure metal ferrites as catalysts remain limited. This project aims to develop cobalt ferrite nanoparticles ($CoFe_2O_4$) using extracts from *Rhizophora mucronata leaves*. The novelty lies in the application of spinel $CoFe_2O_4$ nanospheres for textile pollutant removal through a photoresponsivity process and the inclusion of anti-microbial analysis, potentially leading to more sustainable and efficient methods for reducing pollution and promoting cleaner textile production. (Table 1).

* Corresponding author at: PG and Research Department of Microbiology, Vivekanandha College of Arts and Sciences for Women (Autonomous), Elayampalayam, Namakkal 637205, Tamil Nadu, India.
** Corresponding author at: Department of Allied Health Sciences, Faculty of Science, University Tunku Abdul Rahman, Jalan University, Bandar Barat, Kampar 31900, Malaysia.
E-mail addresses: prasannaj87@gmail.com (J. Prasanna), sinouvassane@utar.edu.my (S. Djearamane).

https://doi.org/10.1016/j.jksus.2024.103369
Received 2 April 2024; Received in revised form 21 July 2024; Accepted 21 July 2024
Available online 23 July 2024

Table 1
Magnetic property of (400 °C) $CoFe_2O_4$ NPs.

Material	Ms (emu/g)	Mr/Ms	Hc (Oe)
Spinel $CoFe_2O_4$	61	0.525	1550

2. Experimental

2.1. Substances

Chemicals were sourced from HI Media-Mumbai, India. The $CoFe_2O_4$ nanoparticles (NPs) were synthesized using ferric nitrate anhydrate (Fe $(NO_3)_3{\cdot}9H_2O$, >99.8 %) and cobalt (II) nitrate hexahydrate (Co $(NO_3)_2{\cdot}6H_2O$, >99.9 %), both of analytical reagent (AR) grade. No additional purification was performed on these reagents. Leaves of the mangrove species *Rhizophora mucronata* were collected from Chinnapalam mangrove, Gulf of Mannar, southeast coast of India, and used as a natural reducing agent due to their nutrient content, which facilitates regulation, stability, and reduction of the core components. The nanoparticles were further processed using double-distilled water.

2.2. Rhizophora mucronata leaf extract preparation

Fresh *R. mucronata leaves (RML)* weighing 100 mg were taken from Chinnapalam mangrove, Gulf of mannar, southeast coast of India. The previously gathered tap water was used to clean the leaves before being extracted via double-distilled water; 100 mg of leaf extract was mixed with 100 ml of distilled water which was subsequently stirred for some time while heating conditions were applied. The resultant mixture was passed through using Whatman No. 1 filter paper, the sample was filtered and then stored at 4 °C for testing (Li et al., 2002).

2.3. Spinel $CoFe_2O_4$ nanosphere synthesis

Spinel $CoFe_2O_4$ nanospheres were synthesized using a simple and environmentally sustainable biotic approach. A solution with a concentration of 0.2 M was prepared by dissolving 13.5 g of iron nitrate and 12.3 g of cobalt nitrate in 200 mL of water. This solution was continuously stirred with a magnetic stirrer. Subsequently, 200 mL of *Rhizophora mucronata leaf* extract was added to the solution. The mixture was stirred for 120 min, leading to the formation of a precipitate. The resulting substance was filtered and rinsed with double-distilled water and ethanol. The precipitate was then dried overnight at 100 °C. The

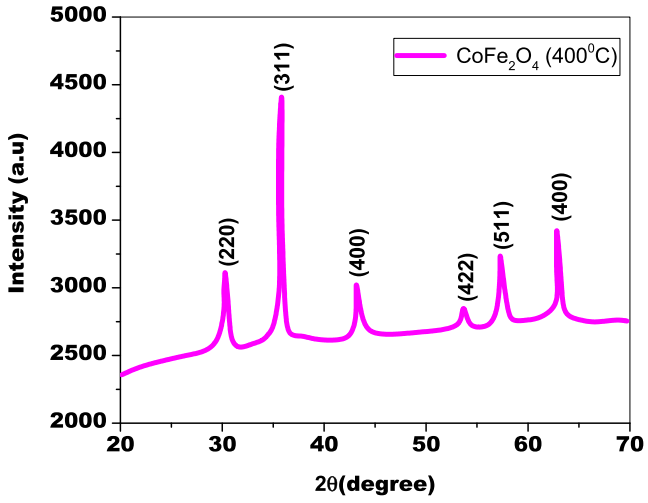

Fig. 2. XRD pattern of as-fabricated $CoFe_2O_4$ nanoparticles by biogenic approach.

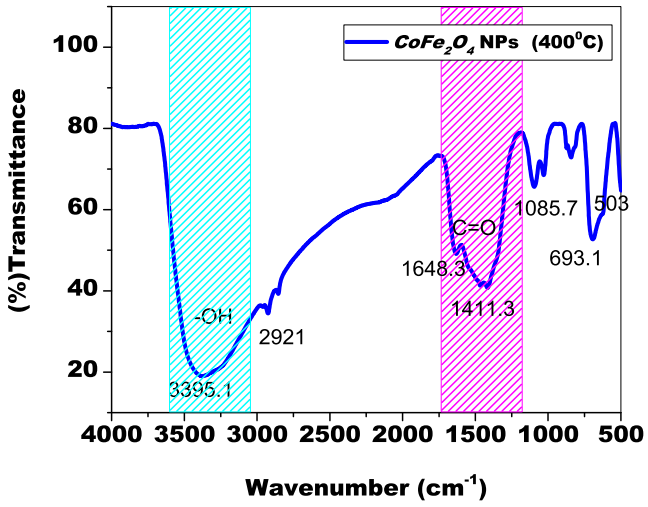

Fig. 3. Functional components of the biosynthesized cofe$_2$O$_4$ nanoparticles.

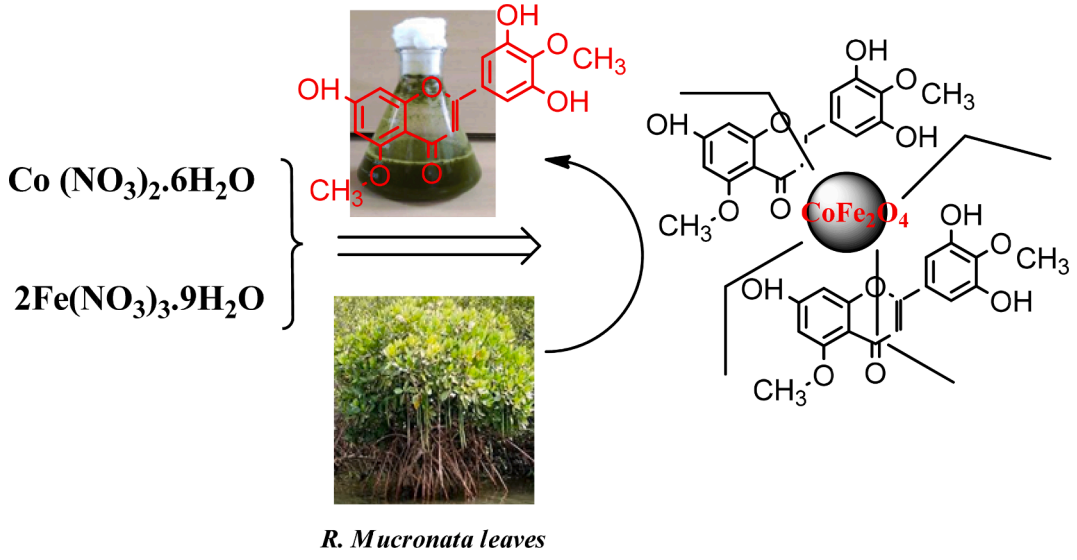

Fig. 1. Reaction pathway of formation of $CoFe_2O_4$ Nanoparticles using mangrove plant species (*R. mucronata leaves* extract).

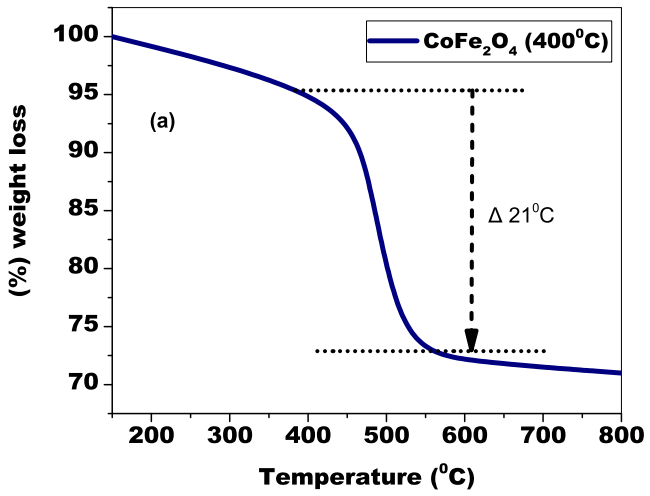

Fig. 4a. Thermal stability of $CoFe_2O_4$ nanocomposites.

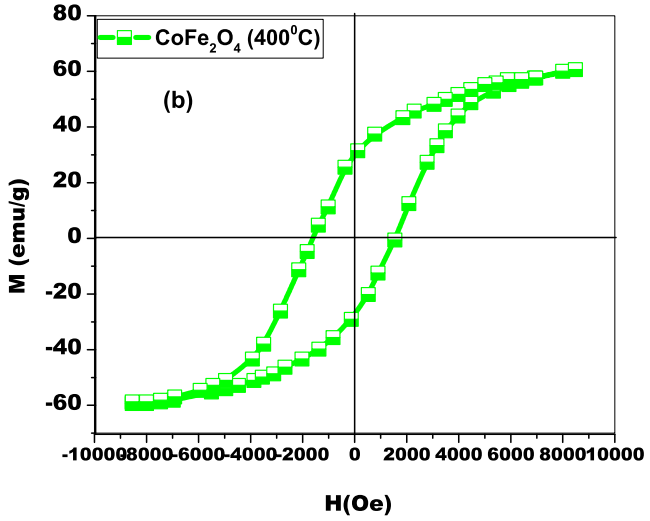

Fig. 4b. M–H curve of $CoFe_2O_4$ NPs using mangrove species.

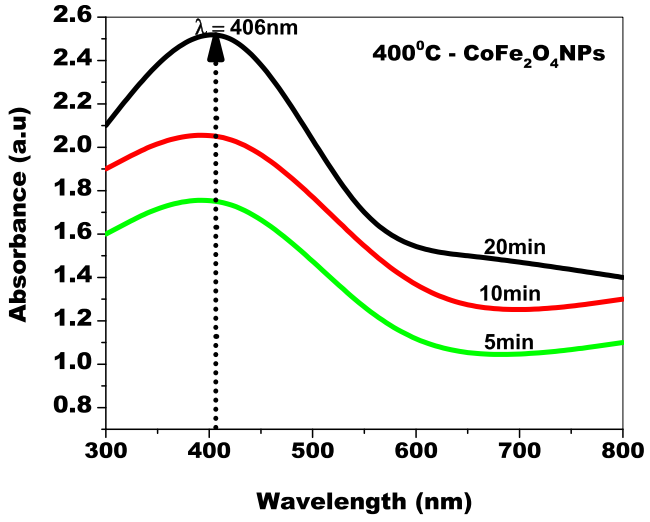

Fig. 5a. UV–Visible absorbance spectrum of $CoFe_2O_4$ NPs by green approach.

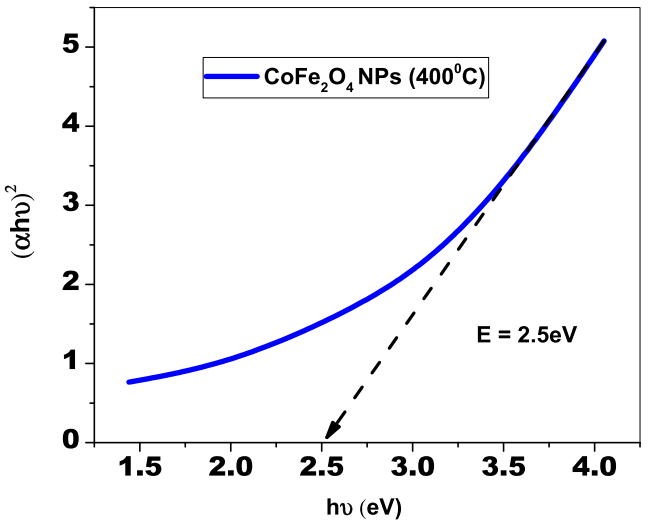

Fig. 5b. Optical band gap of $cofe_2O_4$ nanoparticles by greener synthesis.

dried precipitate was ground into a fine powder and calcined at 400 °C for 180 min. The calcined granules, now designated as $CoFe_2O_4$ NPs were stored in a glass container for further analysis. The reaction pathway for the synthesis of $CoFe_2O_4$ nanoparticles is illustrated in Fig. 1.

2.4. Anti-microbial activity

The antimicrobial properties of the produced $CoFe_2O_4$ nanoparticles (NPs) were assessed using the disc diffusion technique. This method involved testing two bacterial strains, *Staphylococcus aureus and Pseudomonas aeruginosa, and two fungal strains, Candida albicans and Aspergillus niger*. Agar plates inoculated with the bacteria were prepared, and wells of six millimeters in size were made using a sterile plug drill. These wells were then loaded with 200 µg/L of the nanoparticles. The *R. mucronata leaf* extract served as a control. The pathogens were cultured in broth and adjusted to 0.6 according to the McFarland standard. The microorganisms were exposed to 50, 75, and 100 µg/L of the nanoparticles and incubated for 24 h at 37 °C. Each experiment was repeated multiple times, and the average diameters of the inhibition zones were measured in millimeters to evaluate the antimicrobial effectiveness of the nanoparticles.

2.5. Photocatalytic test

The photocatalytic activity of CoFe2O4 nanoparticles was tested by examining the degradation of methylene blue dye under visible light irradiation using a xenon lamp. The process involved combining a 10-ppm solution of 50 mL MB dye with 10 mg of CoFe2O4 NPs, allowing it to sit in the dark for 30 min, then exposed to light for 30 min. to achieve adsorption–desorption equilibrium. To remove the catalyst from the dye solution, the samples were centrifuged at 10,000 rpm for 5 min. The percentage of dye degradation was determined using a formula.

$$(\%)\ \text{degradation} = OD_{control} - OD_{catalyst} / OD_{control} \times 100 \quad (1)$$

where $OD_{control}$ is the initial concentration of the dye, and $OD_{catalyst}$ is the concentration of the dye after irradiation.

3. Results and discussions

3.1. X-ray diffraction analysis

Fig. 2 displays the X-ray diffraction of biosynthesized $CoFe_2O_4$ nanoparticles. The shape of the diffraction pattern illustrates the

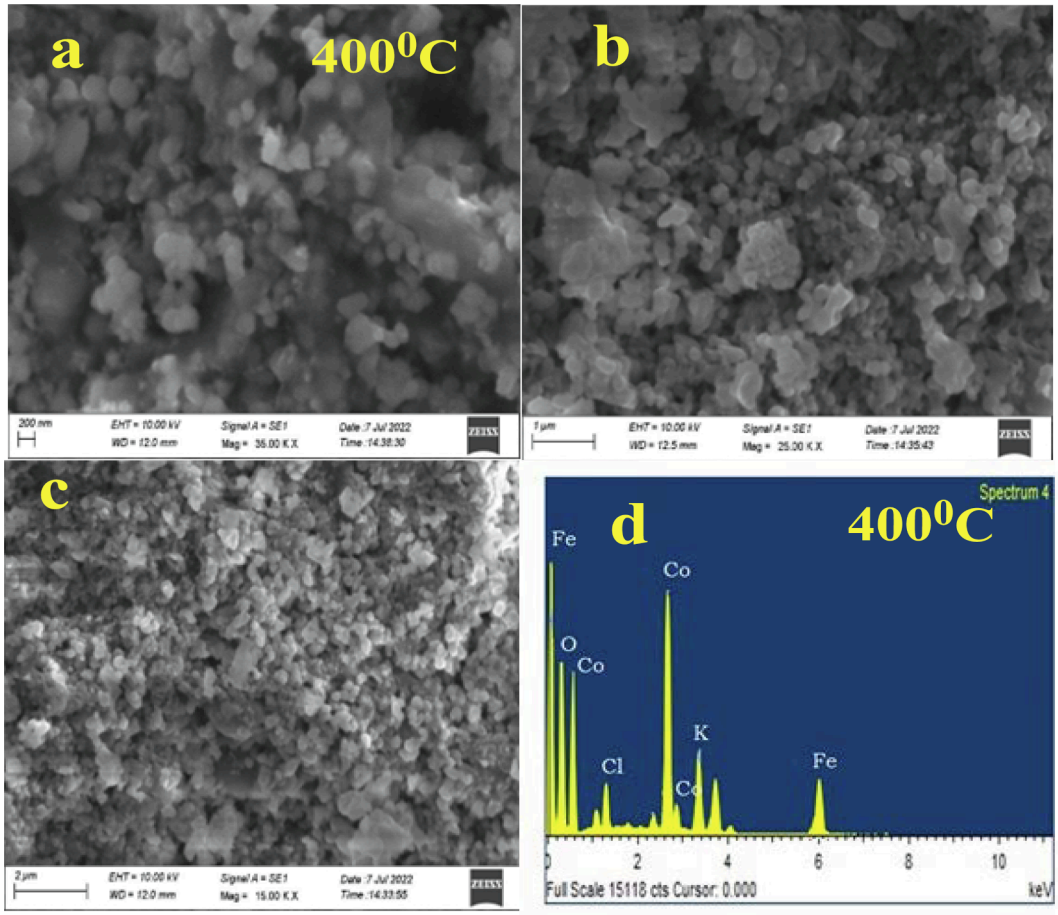

Fig. 6. (a-c) different resolutions of $CoFe_2O_4$ nanoparticles (d) EDX spectrum.

crystallinity and phase structure of biosynthesized $CoFe_2O_4$ nanoparticles. The 2-theta values of the biosynthesized $CoFe_2O_4$ nanoparticles follow the standard cubic phase $CoFe_2O_4$ JCPDS card #22–1086 (Mak et al., 2013; Rana et al., 2015), in addition to their respective positions (*hkl*) plane frequencies are (220), (311), (400), (422), (511), and (400), accordingly. The Debye-Scherrer equation (Basak et al., 2021) was employed to measure the dimension of cubic spinal ferrites of biosynthesized nanoparticles made of $CoFe_2O_4$ crystallite size, which was 24 nm. As a result of their atomic distance (200 pm), ferrites of spinel have been created over cobalt mineral content. The iron-coupled cobalt substances possess tetrahedral sites, while the remaining parts of the iron materials contain spots that are octahedral (Kumar et al., 2015). The amalgamation of the metal's cobalt and iron increased oxygen space, which helped in the development of nanomaterials. The development of nanoparticles was thoroughly established and further developed by the oxygen lattice and their association with materials containing cobalt and iron. Biosynthesized $CoFe_2O_4$ nanoparticles have small crystallite sizes and cubic spinel ferrites can exhibit improved abusing efficiency towards dyes and infections.

3.2. FTIR analysis

The functional components of the biosynthesized $CoFe_2O_4$ tiny particles, along with their decreases as well as the stability inside the title substances, had been identified by employing Thermo-fluorescence infrared spectroscopy; Their FTIR spectrum is as follows in Fig. 3. The substantial peak at 3395 cm^{-1} demonstrates the molecules' –OH stretching surfaces (Das et al., 2015). Observed amides, amines, as well as carbon groups associated with the elimination, limiting, and stability of $CoFe_2O_4$ nanoparticles are represented by the peaks at 1648 cm^{-1}, 1411.3 cm^{-1}, and 1085.7 cm^{-1}. The plant extract's phenolic compounds were employed to construct the Fe-O-Co contact, as well as connections. Peaks of 693 cm^{-1}, 503 cm^{-1}, confirmed the tetrahedral positions of Fe and Co (Rana et al., 2016; Mohamed et al., 2010). Chemicals produced by plants encouraged the generation of ferrites from spinel, which promoted modified breakdown and bio-activities. (Fig. 4a., Fig. 4b.).

3.3. Thermal stability function

Graph 4 (a) depicts the TGA of the elements generated which demonstrates two pounds losses. The process of adsorption water evaporation that occurs on the prepared particle surface contributes to the 21 % reduction in weight between 438–546 K in temperature. The degradation of plant substance and antecedent substance is responsible for the 74 % weight loss at temperatures over 546 K. The modest reduction in weight up to temperature 546 K shows that the catalyst is durable throughout a broad range of temperatures.

3.4. VSM evaluation

The magnetic properties of biosynthesized $CoFe_2O_4$ nanoparticles were studied using Vibrating Sample Magnetometry (VSM), with the results displayed in Fig. 6. The sample exhibited a maximum magnetization (MS) of 61 emu/g, a strong field (HC) of 1550 Oe, and a retentivity (MR) of 32.03 emu/g within the M−H loop. The saturation magnetization achieved is superior to that of bulk cobalt ferrites (MS=81 emu/g) as seen Table 1. This enhanced magnetic attraction confirms the small crystalline framework and strong electromagnetic field of the biosynthesized $CoFe_2O_4$ nanoparticles. The very low

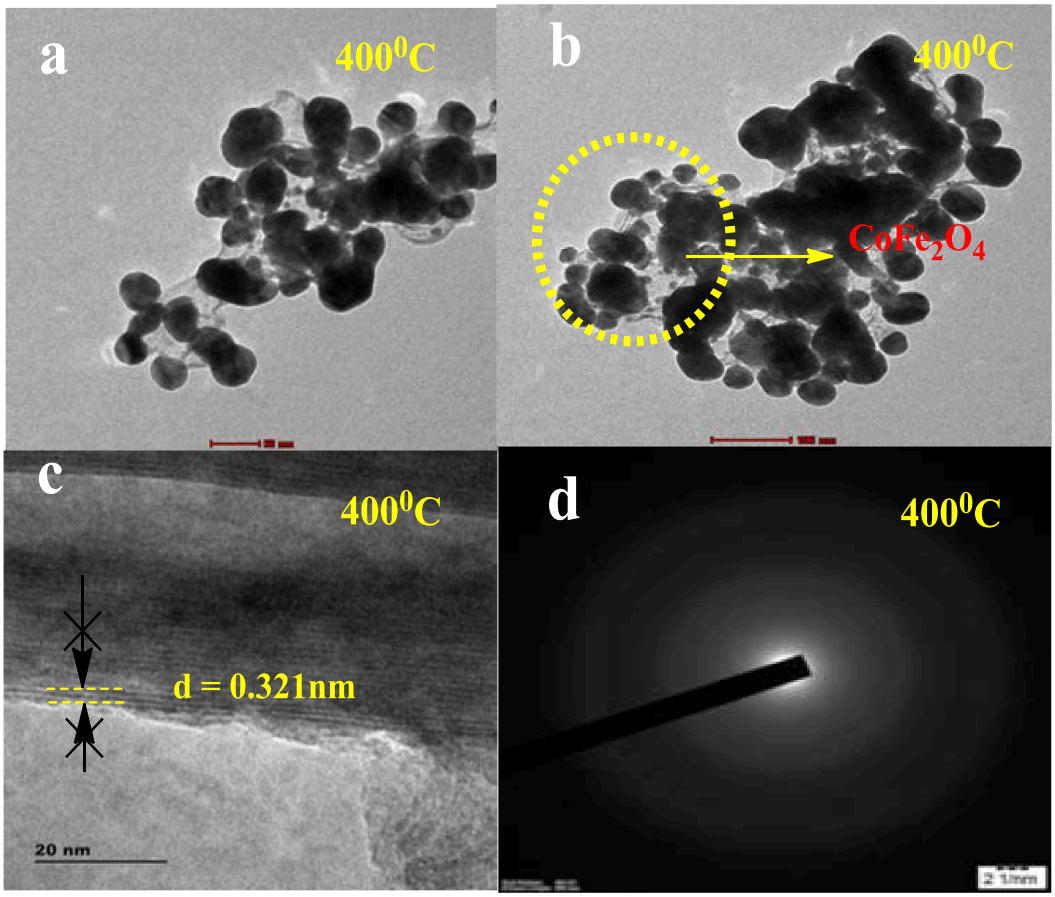

Fig. 7. (a) and (b) different resolution of Morphology (c) HRTEM (d) SAED pattern.

coercivity of the nanoparticles indicates that their magnetic properties are nearing the superparamagnetic limit. At higher fields, the M−H curve shows a straight-line element, suggesting significant influence from paramagnetic forces. These magnetic characteristics imply that biosynthesized $CoFe_2O_4$ nanoparticles can be used for medical applications and are expected to exhibit high catalytic efficiency against harmful organic pollutants (Bohara et al., 2014).

3.5. Optical characterization

Fig. 5a depicts the ultraviolet–visible absorbance spectrum of iron nitrate with pure cobalt nitrate mixtures. The absorbance in the visible region is expressed by cobalt nitrate peaks, whereas the ultraviolet portion of the sensitivity is characterized by iron nitrate peaks. The absorbance of plant leaf extract in its natural state contains chemical compounds, which are visible as a UV absorption peak is quite high area. The ultraviolet (UV) area spike demonstrates that electron molecules possess considerable potential. A small number of plant-based extracts to both nitrate concentrations facilitated electron reduction, whereas Co along with Fe ions as well as their current plant derivatives lowered ions. Furthermore, the spinel metal ferrite structure was formed by lattice oxygen and metal cations.

The optical characteristics were investigated using UV–Visible spectroscopy and flaws of the green-produced $CoFe_2O_4$ tiny particles. As demonstrated in Fig. 5(b), the wavelength of the absorbance peak of $CoFe_2O_4$ tiny particles was positioned at 558 nm, which characterizes $CoFe_2O_4$ nanoparticles' optical entity in the UV range. The ultraviolet (UV) portion of the absorbance spectrum $CoFe_2O_4$ nanoparticles suggest the surface's enhanced electron generation (Tabit et al., 2018). The interaction of plant molecules with cobalt and iron source materials built the electron reduction in the ultraviolet area. $CoFe_2O_4$ nanoparticles' bandgap was computed employing Kubelka-Munk relationship and the corresponding bandgap value of $CoFe_2O_4$ nanomaterials was 2 eV (as shown in Fig. 3b). This small bandgap value provides the best e-h pair combining performance as well as worsening characteristics (Joseph et al., 2017). The bandgap of $CoFe_2O_4$ nanoparticles indicated an extremely small bandgap effect, which has a substantial effect on contaminants made up of organic matter.

3.6. SEM with EDX

EDX analysis was employed to ascertain the outermost form as well as elemental presence within the biosynthesized $CoFe_2O_4$ tiny particles from SEM. Fig. 6 (a–c) demonstrates SEM images of biosynthesized $CoFe_2O_4$ nanoparticles with various levels of magnification The biosynthesized $CoFe_2O_4$ nanoparticles possessed a polydisperse spherical form as well as were uniformly dispersed across the surfaces of the particles. The amount of surface area of spherically structured biosynthesized $CoFe_2O_4$ nanoparticles is significantly greater than that of other forms (Basak et al., 2021). The enhanced breakdown of color and organic contaminants is demonstrated by the spherical form. Fig. 6 (d) depicts the currently available materials of biosynthesized $CoFe_2O_4$ nanoparticles. The elements Co, Fe, and O confirm the substances that were created by title combinations. The biosynthesized $CoFe_2O_4$ nanoparticles possessed more effective morphology, in accordance with SEM and EDX assessment.

3.7. TEM examination

TEM investigation demonstrated surface morphology attributes of

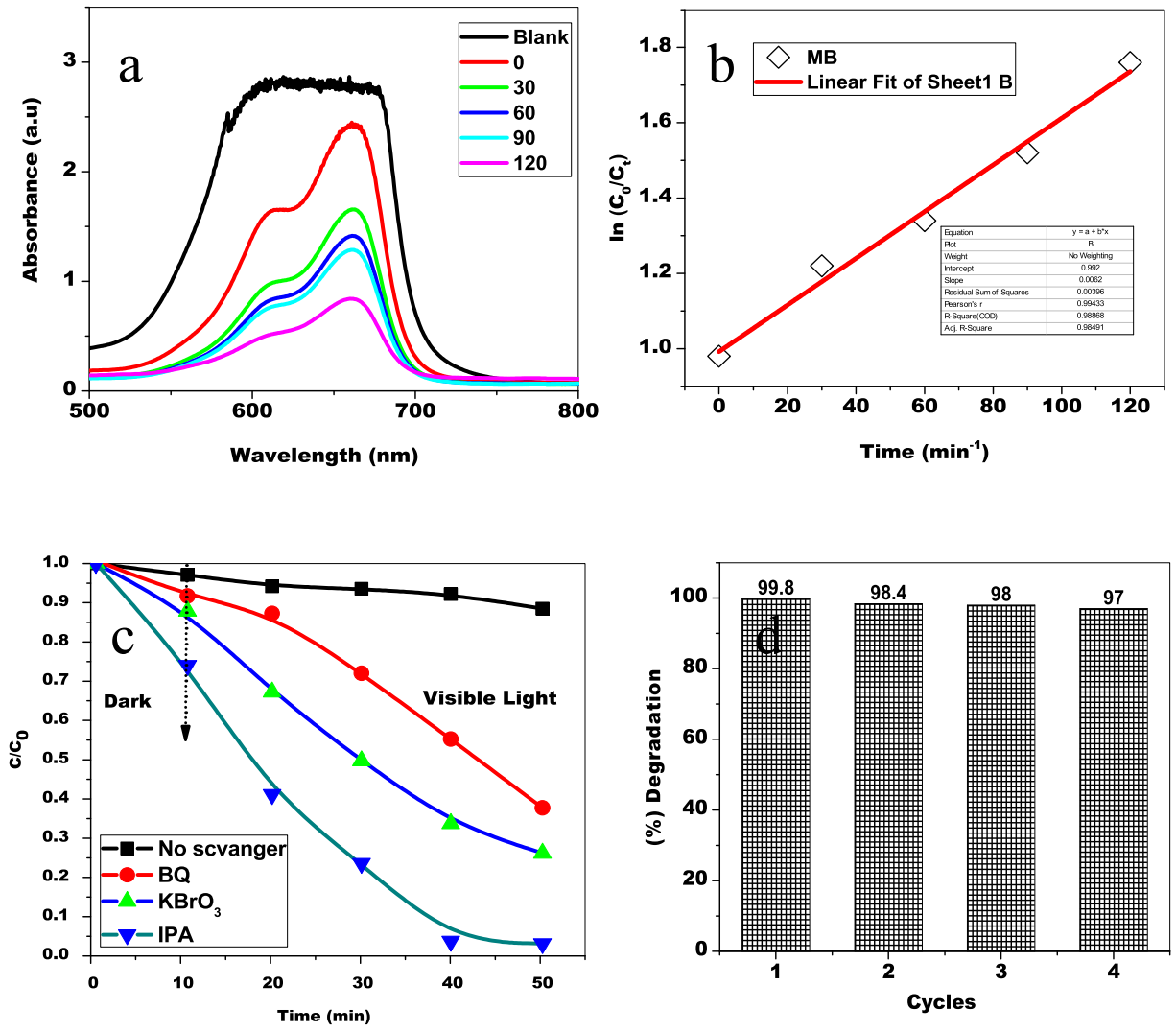

Fig. 8. (a) UV −Visible absorbance spectrum of Methylene Blue degradation (b) Kinetic model (c) scavenger trapping examinations (d) cycling stability.

biosynthesized $CoFe_2O_4$ nanoparticles. Fig. 7 (a) and (b) depicts the various magnified visuals development of biosynthesized $CoFe_2O_4$ nanostructures, The spherical form along with distributions of the biosynthesized $CoFe_2O_4$ nanoparticles were apparent with various magnifications. Fig. 7 (c) demonstrates how biomolecules released on the outermost layer of nanoparticles promote nanoparticle aggregation. The elements cobalt and iron are held together by the oxygen lattice orientated from the substances. The biosynthesized spherical shape $CoFe_2O_4$ nanoparticles has a higher surface area than other shapes and can cause greater degrading activities (Sadegh and Tavakol, 2022). The proposed last-minute spread considering the sphericality of the biosynthesized $CoFe_2O_4$ nanoparticles boosted bacterial strain and organic substance elimination. The biosynthesized nanoparticles of $CoFe_2O_4$ possessed a size of 26 nm, that is extremely near electron accumulation was proportional to the dimension of the crystallite confirmed using UV–Visible assessment. high-resolution transmission investigation demonstrates the emergence across multiple crystal planes of $CoFe_2O_4$ nanoparticles. Following the manufacturing process, nevertheless, the (311) and (400) crystal planes appeared frequently (Fig. 7(d). Fig. 7 (c) illustrates lattice diffusion and overlapping numerous crystal planes, demonstrating the emergence of polycrystalline structures of $CoFe_2O_4$ nanoparticles. Despite the small dimensions, the fragments have been produced in a polycrystalline condition employing SAED (selected-area electron diffraction) is characterized by radially unique rings.

3.8. Photocatalytic activity

The organic dye pollutant MB was used to evaluate the catalytic activity of green-produced $CoFe_2O_4$ nanoparticles when exposed to visible light. MB dye absorption was high in the absence of light, and it diminished frequently for both light and time. The organic MB dye's n-π^* transition was recognized by the minimized transmittance (Fig. 8(a)). The displacement of peaks and decreasing absorbance demonstrate that the MB dye has degraded. The MB dye's smaller absorbance intensity demonstrates disintegration. The fluorescent dye solution's absorbance was evaluated every thirty minutes; a period of 120 min light irradiation across the catalyst's surface outermost layer caused an 84 % decomposition, and when there is no light, the rate of degradation occurred substantially lower (Fig. 8 (a). Because of their suppressed electron-hole combination, as well as their superior biocompatibility, developed magnetic nanoparticles and magnetic ferrites, reactive oxygen species, and biodegradability exhibited microbial growth elimination with catalytic decomposition. Fig. 8 (b) shows that ln(C/C0) = kt, the degradation of a pollutant by $CoFe_2O_4$ nanoparticles can be described using a pseudo-first-order kinetic model with rate constant $k = 0.213\ min^{-1}$.

3.8.1. Light cause mechanism

Fig. 9 shows that whenever light reflected electrons are present in the catalyst solution were triggered from the valence band to the conduction

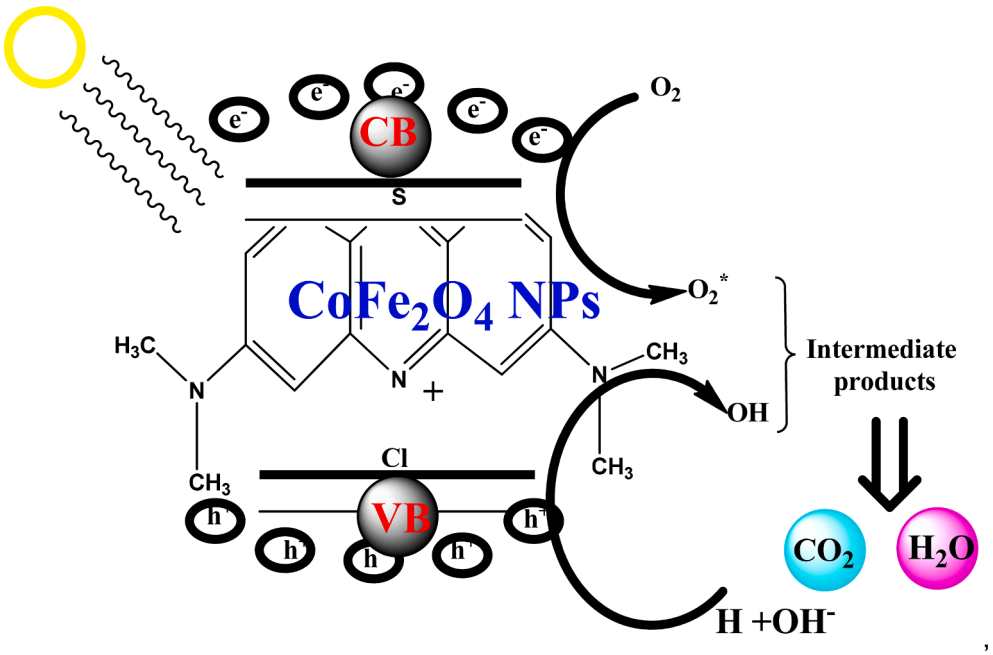

Fig. 9. Photodegradation mechanism of cofe$_2$O$_4$ NPs upon methylene blue dye vis photocatalysis.

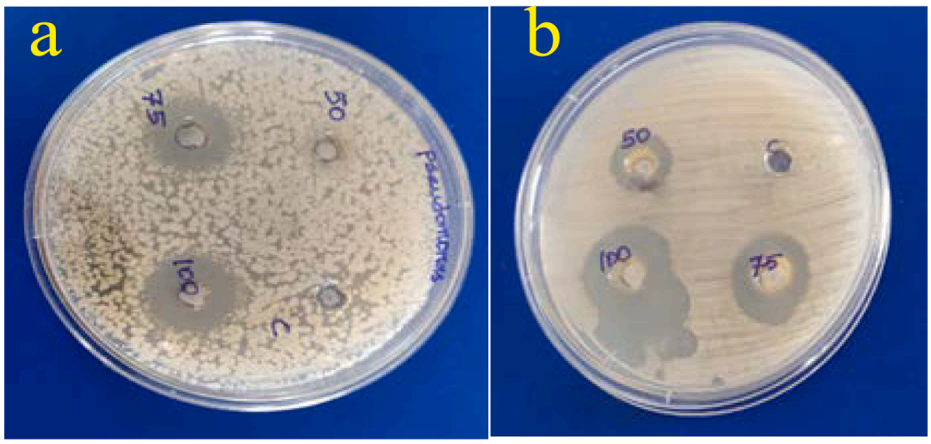

Fig. 10. (a) *P. aeruginosa* and (b) *C. albicans*.

band. e^-/h^+ pair recombination activity is caused by holes in promoted electrons. The oxidation property is generated by the holes, while the reduction property is obtained by the electrons, which leads to super-oxides and hydroxyl radicals as a result. The organic dye compounds become separated and transformed into non-toxic tiny molecules such as CO_2 and H_2O through the use of radicals and super-oxides.

3.8.2. *Trapping experiments*

Under visible light, scavenger trapping examinations were performed to comprehend the photocatalyst oxidation process for the TL and to discover (Fig. 8 (c). Whenever IPA (a radical scavenger) along with $KBrO_3$ (scavenger of electrons) arrived, the oxidation process remained unchanged. In contrast, BQ (superoxide radical anion scavenger) was added had major consequences, whilst the addition of the photocatalytic oxidation process was suppressed by KI (hole scavenger). As a consequence, the holes were the most important oxygen peroxide radicals as the motivator most fundamental photocatalytic oxidation active species mechanism.

3.8.3. *Stability analysis*

The stability and reusability of CoFe2O4 nanoparticles (NPs) as photocatalysts were assessed by repeatedly degrading methylene blue (MB) solution under consistent conditions for four cycles. Despite a slight decrease in degradation efficiency, attributed to catalyst mass loss and dye adsorption on the photocatalyst surface during recycling, the results (Fig. 8 (d)) show that the NPs maintain high photocatalytic performance under visible light irradiation across all cycles. This indicates promising potential for practical applications.

3.9. *Antimicrobial activity*

The Antibacterial efficacy of the purposefully created nanoparticles made from $CoFe_2O_4$ NPs was tested against Gram-positive and Gram-negative pathogens, as well as on fungal species. This is seen in Fig. 10. Therefore, $CoFe_2O_4$ NPs outperformed *RML* extracts (control) in terms of antibacterial activity across every kind of microorganism tested. The zone of inhibition caused by $CoFe_2O_4$ NPs against *S. aureus, P. aeruginosa and fungal species such as C. albicans, and A. niger* was determined to be 18, 19, 28 and 21 mm respectively for 100 µg/L.

Table 2
Anti-microbial analysis of green fabricated $CoFe_2O_4$ NPs using *R. mucronata leaves* extract.

S. No	Tested Pathogens	Zone of inhibition (mm)		
		50 µg/L	75 µg/L	100 µg/L
1	*S. aureus*	05	12	18
2	*P. aeruginosa*	–	18	19
3	*C. albicans*	14	16	28
4	*A. niger*	15	20	21

Table 2 shows that the zone of inhibition of tested pathogens caused by synthesized $CoFe_2O_4$ NPs using *R. mucronata Leaf* extract.

3.9.1. Mechanism

The RML@$CoFe_2O_4$ nanoparticles demonstrated excellent antibacterial activity. Their small size and high surface impact enable them to trap and attract bacterial cells more efficiently than larger particles. The attachment of RML@$CoFe_2O_4$ nanoparticles to the outer layer of the cell membrane disrupts enzyme activity and inhibits DNA replication, ultimately affecting cell permeability and respiration rates (Yao et al., 2022; Kianfar and Fattahi, 2022). This disruption compromises the bacteria's vital processes, leading to effective antibacterial action.

4. Conclusion

This study successfully demonstrated the biosynthesis of $CoFe_2O_4$ nanoparticles using *Rhizophora mucronata leaf* extract as a reducing and stabilizing agent. FTIR analysis confirmed that polyphenolic and other functional groups in the leaf extract are crucial for nanoparticle synthesis. The $CoFe_2O_4$ nanoparticles exhibit enhanced bandwidth, crystallite size, and ferromagnetism, which facilitate electron-hole recombination and radical generation, contributing to the efficiency of the spinel ferrite framework. These biogenic nanoparticles are free from harmful chemicals and do not contribute to pollution. The results show that $CoFe_2O_4$ nanoparticles have improved capabilities in degrading harmful chemicals, and the biogenic approach promotes the formation of chemical-free nanoparticles. The $CoFe_2O_4$ nanoparticles exhibited excellent photocatalytic activity and antimicrobial properties, making them promising candidates for environmental and medical applications.

CRediT authorship contribution statement

M. Abdul Kapur: Methodology, Formal analysis, Data curation. **M. Kaviya Devi:** Formal analysis, Data curation, Conceptualization. **R. Janani:** Software, Resources, Formal analysis, Conceptualization. **J. Prasanna:** Writing – original draft, Validation, Software, Resources, Formal analysis, Conceptualization. **N. Arumugam:** Writing – original draft, Validation, Supervision, Funding acquisition. **Sinouvassane Djearamane:** Writing – original draft, Validation, Software, Resources, Conceptualization. **Ling Shing Wong:** Writing – review & editing, Validation, Supervision, Funding acquisition, Formal analysis, Conceptualization. **Saminathan Kayarohanam:** Resources, Project administration, Funding acquisition, Data curation, Conceptualization.

Declaration of competing interest

The authors declare that they have no known competing financial interests or personal relationships that could have appeared to influence the work reported in this paper.

Acknowledgement

The project supported by PG and Research Department of Microbiology, Vivekanandha College of Arts and Sciences for Women (Autonomous), Elayampalayam, Namakkal, Tamil Nadu, India.

References

Basak, M., Rahman, L., Ahmed, F., Biswas, B., Sharmin, N., 2021. The use of X-ray diffraction peak profile analysis to determine the structural parameters of cobalt ferrite nanoparticles using Debye-Scherrer, Williamson-Hall, Halder-Wagner and Size-strain plot: different precipitating agent approach. J. Alloys Compd. 895, 162694.

Bohara, R.A., Thorat, N.D., Yadav, H.M., Pawar, S.H., 2014. OneStep synthesis of uniform and biocompatible amine func-tionalized cobalt ferrite nanoparticles: a potential carrier for biomedical applications. New J. Chem. 38, 2979–2986.

Charan, C., Shahi, V.K., 2016. Cobalt ferrite (CoFe2O4) nanoparticles (size: ~10 nm) with high surface area for selective non-enzymatic detection of uric acid with excellent sensitivity and stability. RSC Adv. 6, 59457–59467.

Das, R., Kumar, A., Kumar, Y., Sen, S., Shirage, P.M., 2015. Effect of growth temperature on the optical properties of ZnO nanostructures grown by simple hydrothermal method. RSC Adv. 5, 60365–60372.

Issa, B., Obaidat, I.M., Albiss, B.A., Haik, Y., 2013. Magnetic nanoparticles: surface effects and properties related to biomedi-cine applications. Int. J. Mol. Sci. 14, 21266–21305.

Jia, Z., Ren, D., Zhu, R., 2012. Synthesis, characterization and magnetic properties of CoFe2O4 nanorods. Mater. Lett. 66, 128–131.

Joseph, A.M., Thangaraj, B., Gomathi, R.S., Adaikalam, A.A.R., 2017. Synthesis and characterization of cobalt ferrite mag-netic nanoparticles coated with polyethylene glycol. Adv. Nano Biol. M&D. 1, 71–77.

Kavaz, D., Umar, H., Zimuto, T., 2019. Biosynthesis of gold nanoparticles using scytosiphon lomentaria (Brown algae) and spyridia filamentosa (Red algae) from kyrenia region and evaluation of their antimicrobial and antioxidant activity. HJBC. 47 (4), 367–382.

Kavaz, D., Abubakar, A.L., Rizaner, N., Umar, H., 2021. Biosynthesized ZnO nanoparticles using *Albizia lebbeck* extract induced biochemical and morphological alterations in wistar rats. Molecules 26, 3864.

Kianfar, A.H., Fattahi, S., 2022. Synthesis and characterization of magnetically recoverable CoFe2O4 /ZnS/CuO na-noparticles as an effective photocatalyst and catalyst for degradation of MB and reduction of 4-nitrophenol. Appl. Phys. A. 128, 1–14.

Kumar, Y., Rana, A.K., Bhojane, P., Pusty, M., Bagwe, V., Sen, S., Shirage, P.M., 2015. Controlling of ZnO nanostructures by solute concentration and its effect on growth, structural and optical properties. Mater. Res. Express. 2, 105017.

Kumar, Y., Alfa, S.A., Shirage, P.M., 2017. Shape-controlled CoFe2O4 nanoparticles as an excellent material for Hu-midity sensing. RSC Adv. 7, 55778–55785.

Li, X., Chen, G., Po-Lock, Y., Kutal, C., 2002. Preparation and characterization of superparamagnetic nanocrystalline cobalt ferrite materials. J. Mater. Sci. Lett. 21, 1881–1883.

Mak, Y.W., Chuah, L.O., Ahmad, R., Bhat, R., 2013. Antioxidant and antibacterial activities of hibiscus (*Hibiscus rosasinensis* L.) and Cassia (*Senna bicapsularis* L.) flower extracts. J. King Saud Univ. Sci. 25, 275–282.

Malinowska, I., Ryzynska, Z., Mrotek, E., Klimczuk, T., Zielinska-Jurek, A., 2020. Synthesis of CoFe2O4 nanoparticles: the effect of ionic strength, concentration, and precursor type on morphology and magnetic properties. J. Nanomater., 9046219

Mohamed, R., Rashad, M., Haraz, F., Sigmund, W., 2010. Structure and magnetic properties of nanocrystalline cobalt ferrite powders synthesized using organic acid precursor method. J. Magn. Magn. Mater. 322, 2058–2064.

Naseri, M.G., Saion, E.B., Ahangar, H.A., Shaari, A.H., Hashim, M., 2010. Simple synthesis and characterization of cobalt ferrite nanoparticles by a thermal treatment method. J. Nanomater., 907686

Pelino, M., Cantalini, C., Faccio, M., 1994. Principles and applications of ceramic humidity sensors. Act. Passiv. Electron. Components. 16, 69–87.

Rana, A.K., Kumar, Y., Saxena, N., Das, R., Sen, S., Shirage, P.M., 2015. Studies on the control of ZnO nanostructures by wet chemical method and plausible mechanism. AIP Adv. 5, 097118.

Rana, A.K., Das, R., Kumar, Y., Sen, S., Shirage, P.M., 2016. Growth of transparent Zn1−Sr O (0.0 ≤x≤ 0.08) films by facile wet chemical method: effect of Sr doping on the structural, optical and sensing properties. Appl. Surf. Sci. 379, 23–32.

Sadegh, Fatemeh and Tavakol, Hossein, Eco-Friendly Synthesis of a Noble Trimetallic Magnetic Aerogel, Ag/CoFe2O4 , and Employing it as a Catalyst in the Reduction of Nitroaromatics. [(accessed on 21 September 2022).

Shaheen, K., Shah, Z., Khan, B., Adnan, O.M., Alamzeb, M., Suo, H., 2020. Electrical, photocatalytic, and humidity sensing applications of mixed metal oxide nanocomposites. ACS Omega 5, 7271–7279.

Tabit, R., Amadine, O., Essamlali, Y., Dânoun, K., Rhihil, A., Zahouily, M., 2018. Magnetic CoFe2O4 nanoparticles supported on graphene oxide (CoFe2O4 /GO) with high catalytic activity for peroxymonosulfate activation and degradation of rhodamine B. RSC Adv. 8, 1351–1360.

Umar, H., Aliyu, M.R., Usman, A.G., et al., 2023. Prediction of cell migration potential on human breast cancer cells treated with *Albizia lebbeck* ethanolic extract using extreme machine learning. Sci Rep 13, 22242.

Umar, H., Aliyu, MR, Ozsahin, DU, 2024. Iron oxide nanoparticles synthesized using Mentha spicata extract and evaluation of its antibacterial, cytotoxicity and antimigratory potential on highly metastatic human breast cells. Biomed. Phys. Eng. Express 10, 035019.

Yao, K., Zhang, Y., Xu, W., Li, J., Wang, F., Xu, M., Tian, F., Zhou, C., Yang, S., 2022. Exploiting a pronounced photo-magnetic effect over the rational design of facile core–shell ferromagnet. Mater. Lett. 320, 132359.

Further reading

Cannas, C., Falqui, A., Musinu, A., Peddis, D., Piccaluga, G., 2006. CoFe2O4 nanocrystalline powders prepared by citrate-gel methods: synthesis, structure and magnetic properties. J. Nanopartic. Res. 8, 255–267.

Gingasu, D., Mindru, I., Patron, L., Calderon-Moreno, J.M., Mocioiu, O.C., Preda, S., Stanica, N., Nita, S., Dobre, N., Popa, M., et al., 2016. Green synthesis methods of CoFe2O4 and Ag-CoFe2O4 nanoparticles using hibiscus extracts and their antimicrobial potential. J. Nanomater., 2106756